
EditSleuth: A Dataset of Grounded Reasoning Chains for Image-Edit Forensics

Van-Loc Nguyen^{1*}, AprilPyone MaungMaung^{2*}, Minh-Triet Tran¹, Isao Echizen²,

¹University of Science, Vietnam National University Ho Chi Minh City
 {nvloc@selab., tmtriet@}hcmus.edu.vn

²National Institute of Informatics
 {pyone, iechizen}@nii.ac.jp

Abstract

Forensic analysis of AI-edited images requires more than binary real-versus-fake prediction: a useful system should localize the edit, identify its semantic type, and ground its decisions in visual evidence. Existing image-forensics datasets typically emphasize detection or localization, while reasoning-supervised vision-language datasets rarely target image manipulation and often rely on LLM-generated rationales whose faithfulness is difficult to verify. We introduce **EditSleuth**, a dataset of 257,725 image-edit triplets constructed from existing image-editing corpora for grounded image-edit forensic reasoning. Each example includes an edited image, its source image, a binary edit mask, a 12-class edit taxonomy label, a difficulty score, and a six-step reasoning chain. EditSleuth chains are generated deterministically from triplet-grounded upstream artifacts, with each statement tied to a specific computable source of evidence. Our analysis reveals that a naive four-component difficulty formulation suffers from a rank-2 correlation collapse among magnitude features; a simplified three-component formulation substantially increases score dispersion on both Pico-Banana and MagicBrush. Difficulty also varies meaningfully within most edit categories, indicating that the score is not a proxy for edit type. As an initial learning study, we fine-tune Qwen2-VL-2B with LoRA and find that chain-as-target supervision matches a label-only baseline on classification accuracy among parseable answers, while additionally yielding grounded explanatory prose that label-only supervision cannot produce. We release the dataset, the deterministic construction pipeline, and pilot training scripts.

1 Introduction

AI-driven image editing has shifted forensic detection from pixel-level splice and copy-move artifacts to coherent, instruction-conditioned edits that may be subtle, semantic, or globally diffuse. Detecting such edits requires more than binary real-versus-fake classification: a useful forensic system should localize the edit, identify its type, and explain the supporting visual evidence. This gap between modern forensic needs and existing dataset supervision motivates our work.

Two adjacent trends provide useful raw material. First, image-editing datasets such as MagicBrush [Zhang et al., 2023a], InstructPix2Pix [Brooks et al., 2023], UltraEdit [Zhao et al., 2024], EmuEdit [Sheynin et al., 2024], and Pico-Banana [Qian et al., 2025] now offer large-scale (real, edited, instruction) triplets for training editor models. Second, reasoning-supervised VLMs show that chain-of-thought supervision can transfer to multimodal tasks [Chen et al., 2024, Shao et al., 2024, Zhang et al., 2025], but their chains are often generated by frontier LLMs that do not

*Equal Contribution

directly observe the visual evidence, creating an auditability gap. Neither thread directly addresses forensic detection: editing datasets are used to train editors rather than detectors, and reasoning datasets rarely target image manipulation.

EditSleuth bridges these two threads by treating an image-editing triplet $(I_{\text{real}}, I_{\text{edited}}, t_{\text{instr}})$ as a forensic training example. From the image pair, we recover a binary edit mask; from the instruction or source metadata, we recover the edit category; and from these artifacts, we compose a structured reasoning chain whose grounded claims are computed rather than LLM-synthesized. We implement this idea as a five-stage deterministic pipeline that ingests editing triplets, computes edit masks, scores difficulty, assigns one of 12 canonical categories, and emits a six-step reasoning chain in which every triplet-grounded statement traces to a specific upstream artifact. Applied to Pico-Banana single-turn, the pipeline yields 257,725 fully annotated triplets; we also process MagicBrush dev (528 triplets) for held-out cross-instruction-style evaluation.

We characterize EditSleuth and validate its construction through dataset analyses and pilot training. The V2 difficulty formula increases score standard deviation by +55% on Pico-Banana and +94% on MagicBrush by correcting a rank-2 collapse among structural, perceptual, and locality-based magnitude terms. Threshold calibration across LAB+SSIM, LAB+LPIPS, and LAB+LPIPS+SSIM shows that threshold shifts track changes in mean combined diff signal, indicating compensation for max-pool inflation rather than signal-specific artifacts. The category-by-difficulty cross-tab further shows that difficulty varies within most categories, with `geometric` skewing hard (62%) and `text_edit` skewing easy (50%). Finally, a matched-budget pilot fine-tuning study finds that chain-target supervision matches label-only classification quality conditional on parseable outputs, while additionally producing grounded prose. However, chain-target extraction recall remains lower than label-only recall and does not close after one additional epoch.

Contributions. (i) A construction pipeline that re-purposes existing image-editing triplets as forensic-detection training data, with grounded reasoning chains composed deterministically from upstream artifacts. (ii) A 12-category taxonomy of image edits adapted from the Pico-Banana grouping, plus a dataset of $n = 257,725$ triplets populated through the full pipeline, with parallel MagicBrush dev coverage for held-out evaluation. (iii) Empirical validation of the pipeline’s design choices: the rank-2 collapse motivating V2 difficulty, the threshold-calibration observation about max-pool inflation, and the within-category discrimination of the difficulty score. (iv) A pilot fine-tuning study that validates chain-as-target supervision at the classification level and surfaces format conformance as a remaining bottleneck for follow-up work.

2 Related work

EditSleuth lies at the intersection of image-forensics datasets, image-editing datasets, and reasoning-supervised VLM training. We review these threads and use their synthesis to position our contribution.

Image forensics datasets. Image-forensics datasets have developed in two main generations. Early benchmarks for classical manipulations such as splicing and copy-move established the pairing of manipulated images with binary masks localizing edited regions [Dong et al., 2013, Hsu and Chang, 2006, Wen et al., 2016]. These datasets remain important but predate AI-driven editing and provide neither instruction context nor explanations beyond masks. More recent datasets address generative synthesis and editing, benchmarking detectors on AI-generated or AI-edited images [Wang et al., 2023, Chang et al., 2025, Kang et al., 2025, Ji et al., 2026, Ye et al., 2025, Huang et al., 2025, Xu et al., 2025, Wen et al., 2026, Han et al., 2026]. However, most retain a single-label framing, such as real/fake or edit class, without modeling edit localization or the detector’s evidential reasoning. EditSleuth fills this gap by combining masks, category labels, and structured reasoning chains that expose the forensic signals behind each decision.

Image editing datasets. Large-scale image-editing datasets pair a source image, an edit instruction, and the edited result. InstructPix2Pix [Brooks et al., 2023] introduced synthesized edit pairs using language-model-expanded instructions and text-to-image generation. MagicBrush [Zhang et al., 2023a] added human-annotated edits with natural conversational instructions, while later datasets scaled this paradigm with broader generation pipelines and quality controls [Zhao et al., 2024, Sheynin et al., 2024, Hui et al., 2024]. Pico-Banana [Qian et al., 2025] further provides a curated 257K single-turn corpus organized by an edit-type taxonomy. These datasets train editors to map $(I_{\text{real}}, t_{\text{instr}})$ to I_{edited} . EditSleuth re-purposes the same triplets for the reverse task: given $(I_{\text{real}}, I_{\text{edited}}, t_{\text{instr}})$, produce a forensic explanation of the edit.

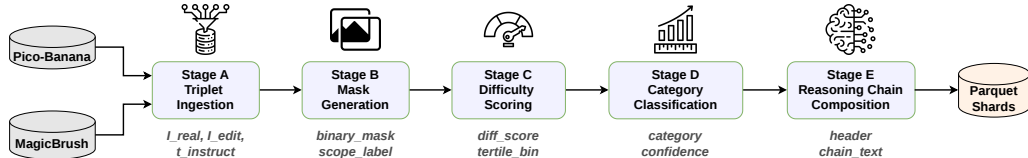


Figure 1: The EditSleuth pipeline. Stage A ingests triplets from source datasets (Pico-Banana [Qian et al., 2025], MagicBrush [Zhang et al., 2023a]) into a unified schema. Stages B–E each consume the previous stage’s output and produce a per-triplet artifact: a binary edit mask (Stage B), a difficulty score (Stage C), a canonical category label (Stage D), and a six-step reasoning chain (Stage E).

Reasoning-supervised VLM training. A third line of work studies how VLMs acquire explicit reasoning. LLaVA-style instruction tuning showed that synthetic instruction-response pairs can produce capable multimodal dialogue [Liu et al., 2023], with later work scaling the approach through larger and more diverse corpora [Liu et al., 2024, Dai et al., 2023]. Recent efforts further introduce explicit reasoning formats, including multimodal chain-of-thought, faithful multimodal reasoning, and visual chain-of-thought supervision [Chen et al., 2024, Zhang et al., 2023b, Li et al., 2025, Shao et al., 2024]. Related work in synthetic-image detection also uses VLMs to generate explanations for AI-generated image forensics [Jiang et al., 2026, Guo et al., 2025, Huang et al., 2025, Wen et al., 2026].

However, two limitations persist. Reasoning chains are often generated by frontier LLMs that do not directly observe the evidence they describe, making fluency easier to guarantee than faithfulness. Their factual claims are also hard to verify at scale without dense annotations. EditSleuth addresses both by composing chains from image-pair-derived artifacts: each triplet-grounded claim traces to a computed upstream value and is auditable end-to-end. Category-level priors are kept separate and marked as category-conditional knowledge.

Positioning. EditSleuth fills the gap between three lines of work. Forensics datasets provide masks and labels but lack instruction context and reasoning chains. Editing datasets provide instruction-conditioned triplets but target image editing rather than forensic explanation. Reasoning-supervised VLM datasets provide chains but often rely on LLM-generated rationales whose faithfulness is difficult to audit. EditSleuth repurposes image-editing corpora for forensic supervision and adds deterministic, artifact-grounded reasoning chains. To our knowledge, it is the first dataset to combine edited-image triplets with auditable reasoning-chain supervision for forensic VLM training.

3 The EditSleuth pipeline

EditSleuth converts existing image-editing datasets into supervised data for image-edit forensics. Given a triplet $(I_{real}, I_{edited}, t_{instr})$ consisting of a source image, its edited counterpart, and the edit instruction, our five-stage pipeline produces a schema-typed record with a binary edit mask, difficulty score, canonical edit category, and structured reasoning chain for downstream VLM supervision (Figure 1). Each stage is deterministic and emits Parquet records joined by a triplet identifier. The Stage E reasoning chains are grounded by construction: triplet-specific claims are computed from upstream artifacts, while category-level forensic priors are explicitly marked. This design makes the chains faithful supervision rather than free-form rationales (§3.4). Stage A handles dataset ingestion through adapters described in Appendix A.

3.1 Stage B: mask generation

Stage B derives a binary edit mask and scope label from each (I_{real}, I_{edited}) pair, where `scope` $\in \{\text{local}, \text{global}, \text{ambiguous}, \text{alignment_failed}\}$. Local masks identify spatially bounded edits, while global masks denote image-wide changes. Qualitative mask examples are in Appendix E.

Multi-signal differencing. We compute three complementary pixel-level difference signals: $L^*a^*b^*$ color distance, structural dissimilarity (1–SSIM), and LPIPS perceptual distance [Zhang et al., 2018]. Each signal is normalized to $[0, 1]$ by its per-pair 99th percentile, then combined by elementwise maximum. This stack captures chromatic, structural, and perceptual edits, improving MagicBrush dev IoU by 1.3 points over the best two-signal subset (paired bootstrap $p < 10^{-4}$, 95% CI $[0.0085, 0.0164]$).

Two-path scope routing. Given the combined diff map $d \in [0, 1]^{H \times W}$, we assign edit scope with a two-path rule. We first route to `global` if $\text{mean}(d) > \tau$, with τ calibrated per dataset. Otherwise, we binarize d using Otsu’s method [Otsu, 1975], apply a small morphological opening, and assign scope by mask area: `global` if $> 90\%$, `local` if $0.5\text{--}90\%$, and `ambiguous` if $< 0.5\%$. Registration failures during $L^*a^*b^*$ computation are logged as `alignment_failed` and propagated downstream. We calibrate τ to target a $\sim 30\%$ global routing rate per dataset ($\tau = 0.62$, 30.4% on Pico-Banana). The full calibration in §5.2 shows that τ offsets across signal-stack variants track offsets in combined diff means, suggesting that calibration mainly compensates for max-pool inflation rather than signal-specific artifacts.

3.2 Stage C: difficulty scoring

Stage C assigns each triplet a scalar difficulty score and tertile bin $\in \{\text{easy}, \text{medium}, \text{hard}\}$ for curriculum sampling and per-difficulty evaluation.

Three-component formula. The production scorer (V2) defines difficulty as

$$D = w_S \cdot s_{\text{struct}} + w_C \cdot s_{\text{compact}} + w_I \cdot s_{\text{instr}}$$

with default weights $(w_S, w_C, w_I) = (0.55, 0.25, 0.20)$. The components measure edit magnitude, spatial dispersion, and instruction complexity:

$$s_{\text{struct}} = 1 - \text{SSIM}(I_{\text{real}}, I_{\text{edited}}),$$

$$s_{\text{compact}} = 1 - \text{compactness}(M), \quad \text{compactness}(M) = \sqrt{\frac{|M|}{|\text{bbox}(M)|} \cdot \frac{|M_{\text{largest cc}}|}{|M|}},$$

where M is the Stage B binary mask, and s_{instr} is a heuristic score based on instruction length, verb count, conjunction count, and spatial-reference count.

The choice of three components rather than V1, four (structural, perceptual, locality, instruction) follows from a correlation-structure observation: the magnitude trio collapses to rank-2 on both datasets (pairwise $|r| \in [0.68, 0.91]$), suppressing the variance of the combined score under weighted summation. V2 retains s_{struct} as the magnitude representative and adds compactness as a genuinely independent spatial signal, widening the score’s standard deviation by $+94\%$ on MagicBrush and $+55\%$ on Pico-Banana relative to the four-component baseline (§5.1).

Tertile binning. We compute the empirical 33rd and 66th percentiles of D on each dataset and bin triplets accordingly. Binning is dataset-internal so that `easy/medium/hard` labels remain meaningful relative to corpus statistics rather than absolute thresholds.

3.3 Stage D: category classification

Stage D assigns each triplet a canonical edit-category label drawn from a 12-category taxonomy: `object_addition`, `object_removal`, `object_replacement`, `attribute_change`, `style_transfer`, `photometric`, `scene_transformation`, `background_change`, `text_edit`, `geometric`, `human_centric`, and an explicit other bucket.

Taxonomy choice. Our taxonomy adapts the eight-category Pico-Banana grouping [Qian et al., 2025] with three changes. First, we separate `photometric` edits from `style_transfer`, since global tone, grain, and color shifts have different forensic signatures from structural texture rewrites. Second, we add `human_centric` for 14 person-specific, identity-preserving operations, including pose, expression, clothing, Funko-Pop, and LEGO-style edits. Third, we keep `background_change` distinct from `scene_transformation` to capture foreground-preserving background swaps present in MagicBrush but absent from Pico-Banana’s taxonomy.

Two-path classification. Stage D assigns edit categories through either source-label mapping or instruction-based rules. For datasets with per-row labels, such as Pico-Banana’s `source_edit_type`, we use a hand-curated lookup covering all 35 distinct Pico-Banana labels. For instruction-only datasets, such as MagicBrush, we apply an ordered regex classifier over explicit edit verbs, conversational frames, domain keywords, and geometric operations. Each prediction records its `source` and `confidence`; unmapped cases route to `other` with the original string preserved for audit. Pico-Banana classifies entirely through the label path with zero `other`, while MagicBrush dev reaches 56% rule coverage, leaving 44% as `other` (§6).

3.4 Stage E: reasoning chain composition

Stage E generates the per-triplet reasoning target for downstream VLM training: a structured one-line header for filtering and a six-step prose chain used as the supervised output.

The faithfulness model. EditSleuth separates two statement types by construction. *Triplet-grounded statements* describe the current example and are sourced from upstream artifacts: the instruction from Stage A, localization and area from Stage B, structural-change and compactness scores from Stage C, and category label and confidence from Stage D. *Category-level priors* describe typical forensic signatures for the predicted edit type, using one of 12 hand-curated templates. Priors are explicitly hedged (e.g., “Edits of this type *typically* exhibit...”) so models distinguish per-triplet evidence from category-conditional knowledge.

A naive LLM-based approach could produce fluent but unsupported rationales. In contrast, template-driven composition only states claims licensed by upstream artifacts, making numerical and categorical claims auditable end-to-end. Faithfulness is thus artifact-relative: upstream biases, such as residual structural-compactness correlation (§5.1), propagate into the chains and are documented.

Chain structure. Each chain contains six numbered steps (~80–150 words): (1) the quoted edit instruction; (2) spatial localization using a coarse descriptor from {`whole_image`, `four quadrants`, `centered`, `scattered`, `alignment_failed`}; (3) magnitude from structural-change and compactness scores; (4) edit category and classification source; (5) category-level forensic prior; and (6) difficulty bin and score. The fixed order provides uniform supervision, while each step is instantiated from triplet-specific artifacts. Full per-category examples of reasoning chains appear in Appendix D.

The 12 forensic-prior templates are listed in Appendix B. Each specifies category-relevant forensic cues, such as boundary discontinuities, lighting inconsistencies, inpainting artifacts, global histogram shifts, and font-rendering noise.

4 Dataset characterization

We characterize EditSleuth by scale and category coverage (§4.1), mask-derived spatial properties (§4.2), and difficulty distribution (§4.3). Results come from one pipeline run on the Pico-Banana single-turn corpus [Qian et al., 2025], our primary training source, with MagicBrush dev [Zhang et al., 2023a] as a smaller held-out comparison.

4.1 Scale and category coverage

The Pico-Banana derivation yields 257,725 triplets, each with a binary edit mask (Stage B), difficulty score, and tertile bin (Stage C), canonical edit category (Stage D), and six-step reasoning chain (Stage E). One corrupted source pair was dropped during Stage B, with no additional downstream loss. The parallel MagicBrush dev split contains 528 triplets processed through the same pipeline and is used for held-out inspection and cross-dataset analysis.

Table 1 reports per-category counts. Pico-Banana covers all 11 non-other categories, with no category above 21% and the smallest non-zero category, `text_edit`, at 4.1%. Its `other` bucket is empty because the source taxonomy maps fully to our canonical labels. MagicBrush dev covers a different subset, dominated by object additions and attribute changes, with smaller removal, replacement, and `background_change` groups. Its 44.5% `other` rate reflects the limits of regex classification on free-text conversational instructions (§6).

The two corpora play complementary roles. Pico-Banana provides a large, taxonomically curated training source, while MagicBrush serves as a smaller held-out set with naturally phrased instructions for testing generalization to a different instruction style. We therefore do not merge them into a single training pool.

4.2 Spatial properties of the edits

Stage B classifies 30.4% of Pico-Banana triplets as `global` and 69.6% as `local`. `photometric` and `style_transfer` edits are global by construction, while `scene_transformation` is mostly global because weather, lighting, and seasonal changes affect the full scene. Object-level categories and `human_centric` edits are predominantly local, with masks concentrated on the modified region.

For local triplets, Stage E assigns a coarse spatial descriptor: one of four quadrants, `centered`, or `scattered`. On Pico-Banana, the distribution is highly skewed: `centered` covers 89% of local edits, quadrants account for only ~5% in total (1.0–1.8% each), and `scattered` covers 5.5%. This

Table 1: Per-category triplet counts and within-category difficulty distributions. The left block reports counts for each source dataset: Pico-Banana uses curated dataset labels, while MagicBrush uses rule-based classification. The right block reports Pico-Banana within-category difficulty distributions, with rows summing to 100%. `background_change` is reserved for foreground-preserving background swaps, which appear in MagicBrush but not Pico-Banana; categories with zero Pico-Banana coverage have undefined difficulty distributions and are marked “—”. `geometric` edits skew hard, while localized `text_edit` examples skew easy.

Category	Pico-Banana		MagicBrush dev		Difficulty (Pico-Banana, %)		
	count	%	count	%	easy	medium	hard
<code>object_addition</code>	14,187	5.5	151	28.6	37.4	35.8	26.8
<code>object_removal</code>	15,109	5.9	42	8.0	37.6	36.9	25.6
<code>object_replacement</code>	14,547	5.6	26	4.9	41.2	35.5	23.3
<code>attribute_change</code>	24,600	9.5	49	9.3	38.3	32.4	29.3
<code>style_transfer</code>	42,871	16.6	0	0.0	31.1	36.1	32.8
<code>photometric</code>	30,188	11.7	0	0.0	43.8	31.4	24.8
<code>scene_transformation</code>	52,691	20.4	7	1.3	32.3	34.8	32.9
<code>background_change</code>	0	0.0	11	2.1	—	—	—
<code>text_edit</code>	10,688	4.1	5	0.9	50.4	30.6	19.0
<code>geometric</code>	32,742	12.7	2	0.4	12.8	25.2	62.0
<code>human_centric</code>	20,102	7.8	0	0.0	31.6	36.4	32.0
<i>other</i>	0	0.0	235	44.5	—	—	—
total	257,725	100	528	100			

reflects Pico-Banana’s curated, subject-centered imagery rather than a descriptor artifact. We retain the descriptor for faithfulness, while preserving mask area fraction as the more informative spatial signal in Step 2 of the reasoning chain.

4.3 Difficulty distribution

The Stage C V2 score on Pico-Banana has a mean of 0.450 and standard deviation of 0.109, with tertile cutoffs at 0.406 and 0.504. By construction, tertile binning produces 85,909 `easy`, 85,908 `medium`, and 85,908 `hard` triplets. Component statistics show that difficulty is driven mainly by structural change and compactness: s_{struct} has $\mu = 0.446$, $\sigma = 0.244$; s_{compact} has $\mu = 0.323$, $\sigma = 0.258$; and s_{instr} has $\mu = 0.621$, $\sigma = 0.108$.

Table 1 reports within-category difficulty bins. `geometric` edits, including zoom, outpainting, and object relocation, skew strongly hard (62.0%) because canvas-level transformations increase both structural change and mask dispersion. In contrast, `text_edit` skews easy (50.4%), reflecting its typically small, localized changes with modest structural impact.

The other nine categories are more evenly distributed, with no bin exceeding $\sim 40\%$ within a category. This reflects broad within-category variation: an object addition may be a small accessory or a large scene element, while a photometric edit may range from a subtle tone shift to a strong filter. This spread shows that difficulty is not merely a proxy for category; instead, it provides an additional curriculum axis by discriminating edit magnitude within most categories.

We qualitatively validated the bins by inspecting a stratified sample of ~ 50 Pico-Banana triplets. Clear, well-localized edits typically fell in `easy` or `medium`, while saturated whole-image masks or visually diffuse edits fell in `hard`. This pattern held across categories, consistent with the cross-tab evidence that most categories span the difficulty range.

The category-by-difficulty distribution supports two downstream uses. First, curriculum sampling can stratify jointly by category and difficulty, exposing models to both local edits and challenging global transformations throughout training. Second, the reported marginals provide a natural evaluation breakdown: strong performance on `easy text_edit` but weak performance on `hard geometric` implies a different failure mode than uniform performance across the joint distribution.

5 Experiments

We validate EditSleuth along four axes: difficulty-score ablations against a four-component baseline (§5.1), threshold calibration across signal stacks and datasets (§5.2), qualitative inspection of rea-

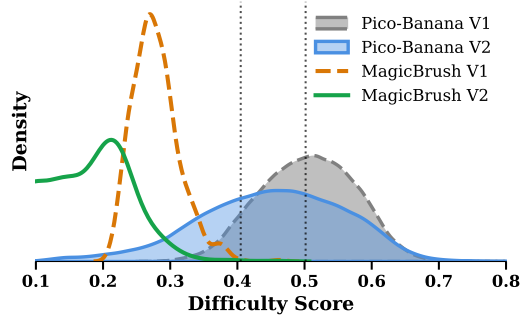


Figure 2: V1 vs V2 difficulty score distributions, side-by-side, on Pico-Banana ($n = 257,725$) and MagicBrush dev split ($n = 528$). V2 widens the standard deviation by +55% ($\sigma_{V1} = 0.070, \sigma_{V2} = 0.109$) and produces tertile bins separated by $\sim 1\sigma$ rather than by margins below noise.

Table 2: Per-stack calibrated thresholds on Pico-Banana ($n = 257,725$). Threshold offsets closely track shifts in the mean combined diff signal (cdm.mean), suggesting that τ primarily compensates for max-pool inflation rather than signal-specific artifacts.

Signal stack	cdm.mean	calibrated τ	Path-1 rate (%)
LAB + SSIM	0.429	0.52	28.4
LAB + LPIPS	0.465	0.56	29.1
LAB + LPIPS + SSIM	0.530	0.62	30.4

soning chains (§5.3), and a pilot fine-tuning comparison between chain supervision and label-only training (§5.4).

5.1 Difficulty formula ablation

V2 collapses the magnitude trio (structural change, perceptual change, locality) of the four-component baseline (V1) into its single canonical representative (s_{struct}) and adds mask compactness as an independent spatial term (§3.2). We score the same Stage B outputs with both formulas, computing tertile bins separately for each scorer, on Pico-Banana ($n = 257,725$) and MagicBrush dev ($n = 528$).

Variance widening. V2 increases score standard deviation by +94% on MagicBrush (0.034 \rightarrow 0.066) and +55% on Pico-Banana (0.070 \rightarrow 0.109). The larger MagicBrush gain reflects stronger V1 rank collapse: magnitude-term correlations are [0.78, 0.91] on MagicBrush versus [0.68, 0.85] on Pico-Banana.

Why the trio collapses. The collapse is driven by the strong negative correlation between $s_{\text{loc}} = 1 - \text{mask_area_frac}$ and the two magnitude terms. Large edits raise s_{struct} and s_{perc} but lower s_{loc} because the mask area grows, causing partial cancellation in the weighted sum. This compresses the combined score to roughly 1/4–1/5 of a single component’s variance. V2 avoids this by using one canonical magnitude term and adding compactness, which is more independent of edit magnitude.

One residual issue remains: on Pico-Banana local edits, V2’s image-derived components, s_{struct} and s_{compact} , show a moderate negative correlation ($r = -0.44$). This likely reflects Stage B mask-quality artifacts, where subtle diffs produce noisier, less compact masks. We discuss this limitation and propose image-pair embedding distance as a future third component in §6.

5.2 Threshold calibration across signal stacks

Stage B uses a per-dataset threshold τ on the mean combined diff signal for Path-1 global routing. We compare three signal stacks—LAB+SSIM, LAB+LPIPS, and LAB+LPIPS+SSIM—and calibrate τ to produce a $\sim 30\%$ Path-1 global rate on Pico-Banana. This target matches the share of Pico-Banana labels corresponding to whole-image edits, including style transfer, photometric overlays, scene transformations, and geometric canvas operations.

Max-pool inflation. Threshold offsets between signal stacks closely track shifts in mean combined diff: +0.04 from LAB+SSIM to LAB+LPIPS versus +0.036 in cdm.mean, and +0.06 from

Table 3: Pilot fine-tuning results on MagicBrush dev ($n = 528$).

Field	Chain target		Label-only	
	accuracy	extracted	accuracy	extracted
category	22.5%	67.4%	37.1%	93.6%
spatial descriptor	29.7%	79.9%	42.2%	100%
difficulty bin	28.0%	68.6%	33.1%	100%
joint (all 3)	1.9%	—	3.4%	—

LAB+LPIPS to LAB+LPIPS+SSIM versus $+0.065$. This reflects elementwise max-pooling, which monotonically increases the per-pair diff mean; τ must rise accordingly to preserve a fixed routing rate. Thus, thresholds do not transfer across stacks directly, but their adjustment is predictable from the `cdm.mean` shift. Appendix C provides a retrospective threshold sweep tool.

5.3 Qualitative chain inspection

We inspect a stratified sample of ~ 50 Pico-Banana triplets across difficulty bins, checking whether triplet-grounded numerical claims match upstream artifacts and whether category-level forensic priors match the visible edit.

We find no faithfulness violations: all numerical claims, including mask area fraction, structural-change score, and difficulty bin, match upstream artifacts by construction. Forensic priors are visually plausible except in two MagicBrush cases where keyword rules misclassified the edit semantics. On Pico-Banana, where categories come from curated labels, priors are always appropriate. Appendix D shows per-category examples.

5.4 Pilot fine-tuning study

We run a small pilot to compare chain supervision with label-only training. The study uses one base VLM, one fine-tuning setup, and one held-out evaluation; larger-scale training is left to follow-up work.

Setup. We fine-tune Qwen2-VL-2B-Instruct [Wang et al., 2024] with LoRA [Hu et al., 2022] ($r = 16$, $\alpha = 32$; target modules $\{q_proj, v_proj\}$ in language layers) on a stratified Pico-Banana subset ($n_{\text{train}} \sim 20,000$), balanced across 11 non-`other` categories and three difficulty bins. We compare two variants with identical base model, hyperparameters, and step budget: *chain-target*, which predicts the full Stage E reasoning chain, and *label-only*, which predicts a JSON `{category, scope, difficulty_bin}` triple. Evaluation uses MagicBrush dev ($n = 528$) for held-out cross-instruction-style generalization; MagicBrush is never seen during training.

Metrics. We report category, spatial-descriptor, difficulty-bin, and joint accuracy on the held-out set, counting unextractable predictions as incorrect. We also report field-extraction recall, i.e., the fraction of generations from which each field can be parsed. For the chain-target model, we extract category, spatial descriptor, and difficulty bin from steps 4, 2, and 6, respectively; for the label-only model, we parse all fields directly from JSON.

Results. Table 3 compares both training configurations on MagicBrush dev across the four evaluation metrics.

Label-only achieves higher raw per-field accuracy, mainly because its extraction recall is much higher ($\sim 94\text{--}100\%$ vs. $\sim 67\text{--}80\%$ for chain-target). Conditional on successful extraction, chain-target obtains $33.4\%/37.2\%/40.8\%$ on category/spatial/bin, compared with label-only’s $39.7\%/42.2\%/33.1\%$. Thus, chain-target matches or exceeds label-only on two of three fields once parseability is controlled for; the raw gap is driven primarily by less frequent parseable outputs rather than weaker classification.

Absolute accuracies are limited by noisy MagicBrush dev labels: the set lacks curated category annotations, so “ground truth” comes from the same rule classifier with a 44% fallback rate (§4.1). Manual inspection reveals several questionable label assignments. Thus, the relative model comparison is more reliable than the absolute accuracy values.

Effect of additional training. A two-epoch re-run with the same hyperparameters does not close the recall gap. Label-only improves modestly (category $37.1 \rightarrow 39.6\%$, bin $33.1 \rightarrow 34.7\%$) with

recall near 100%, while chain-target regresses: spatial extraction recall drops $79.9 \rightarrow 67.0\%$, and conditional spatial/bin accuracy falls from $37.2 \rightarrow 32.5\%$ and $40.8 \rightarrow 34.4\%$. Six-step chain format conformance is therefore harder to learn than JSON output, and the 2B LoRA model appears to plateau below label-only recall.

Interpretation. When outputs are parseable, chain-target supervision matches label-only training on category, spatial, and difficulty classification, indicating no loss in underlying prediction quality. Its added benefit is grounded prose: all chain-target generations include evidence such as mask area, structural-change score, and category-level forensic priors, which label-only training cannot produce. The main limitation is format conformance, which does not improve with one additional epoch at this scale and likely requires a larger model, more diverse data, or explicit conformance training.

6 Limitations and broader impact

Limitations. We flag six limitations of the dataset and the pilot.

- *Residual mask-quality coupling.* On Pico-Banana local edits, V2’s image-derived components remain moderately anti-correlated ($r = -0.44$; §5.1) because subtle edits yield noisier, less compact masks. Future work may replace compactness with image-pair embedding distance.
- *Rule-coverage gap on MagicBrush.* Stage D assigns 44% of MagicBrush dev triplets to other (§4.1), reflecting the limits of regex rules on conversational instructions. We therefore use MagicBrush as a held-out evaluation rather than training data.
- *Single-source training corpus.* Pico-Banana is generated by one text-conditioned editor, so Stage B masks reflect that editor’s artifact statistics. Models trained on EditSleuth may transfer imperfectly to edits from other generators.
- *Artifact-relative faithfulness.* Chains are auditable against upstream masks, difficulty scores, and category labels, but these artifacts are themselves outputs of computational stages. A small human-annotated audit set is a natural next step.
- *Pilot scope.* The fine-tuning pilot (§5.4) uses one 2B VLM with LoRA, a $\sim 20\text{K}$ stratified subset, and MagicBrush dev evaluation. A two-epoch follow-up does not close the chain-target recall gap, suggesting that better format conformance likely requires a larger model, more diverse data, or explicit conformance training.
- *Unverified inference-time chain faithfulness.* The pilot model learns to emit six-step chains, including numerical fields, but does not compute those fields from the underlying artifacts. Thus, generated triplet-grounded statements are model estimates rather than verified quantities; measuring this drift remains open.

Broader impact. EditSleuth has dual-use implications. Positively, it can support forensic detectors for image authentication in journalism, legal evidence, and content moderation; its grounded reasoning chains improve audibility relative to black-box classifiers. Negatively, such detectors could suppress legitimate creative work or intensify an arms race in which generators learn to avoid the forensic cues encoded in our templates. We therefore release EditSleuth under a research-use license and recommend human-in-the-loop deployment, especially in high-stakes settings.

7 Conclusion

We introduced EditSleuth, a dataset and pipeline that converts image-editing triplets into forensic supervision with edit masks, difficulty scores, category labels, and deterministic six-step reasoning chains grounded in upstream artifacts. Three construction findings stand out. First, V2 increases difficulty-score standard deviation by +55% on Pico-Banana and +94% on MagicBrush by replacing a rank-collapsed magnitude trio with one canonical magnitude term plus compactness (§5.1). Second, threshold offsets across signal stacks track combined-diff means, showing that calibration mainly corrects max-pool inflation rather than signal-specific quirks (§5.2). Third, the category-by-difficulty cross-tab shows that difficulty varies within most categories, with `geometric` skewing hard (62%) and `text_edit` skewing easy (50%) (§4.3). Two follow-up directions remain. First, the pilot should be scaled beyond one base VLM, one LoRA setup, and one held-out evaluation, with emphasis on closing the chain-target extraction-recall gap (§5.4). Second, a small human-annotated audit set is needed to evaluate upstream artifact correctness and move the faithfulness guarantee from artifact-relative to ground-truth-relative. We release the dataset, construction pipeline, and pilot training scripts under a research-use license.

References

- Kai Zhang, Lingbo Mo, Wenhui Chen, Huan Sun, and Yu Su. Magicbrush: A manually annotated dataset for instruction-guided image editing. *Advances in Neural Information Processing Systems*, 36:31428–31449, 2023a.
- Tim Brooks, Aleksander Holynski, and Alexei A Efros. Instructpix2pix: Learning to follow image editing instructions. In *Proceedings of the IEEE/CVF conference on computer vision and pattern recognition*, pages 18392–18402, 2023.
- Haozhe Zhao, Xiaojian Ma, Liang Chen, Shuzheng Si, Rujie Wu, Kaikai An, Peiyu Yu, Minjia Zhang, Qing Li, and Baobao Chang. Ultraedit: Instruction-based fine-grained image editing at scale. *Advances in Neural Information Processing Systems*, 37:3058–3093, 2024.
- Shelly Sheynin, Adam Polyak, Uriel Singer, Yuval Kirstain, Amit Zohar, Oron Ashual, Devi Parikh, and Yaniv Taigman. Emu edit: Precise image editing via recognition and generation tasks. In *Proceedings of the IEEE/CVF Conference on Computer Vision and Pattern Recognition*, pages 8871–8879, 2024.
- Yusu Qian, Eli Bocek-Rivele, Liangchen Song, Jialing Tong, Yinfei Yang, Jiasen Lu, Wenze Hu, and Zhe Gan. Pico-banana-400k: A large-scale dataset for text-guided image editing. *arXiv preprint arXiv:2510.19808*, 2025.
- Qiguang Chen, Libo Qin, Jin Zhang, Zhi Chen, Xiao Xu, and Wanxiang Che. M3cot: A novel benchmark for multi-domain multi-step multi-modal chain-of-thought. In *Proceedings of the 62nd Annual Meeting of the Association for Computational Linguistics (Volume 1: Long Papers)*, pages 8199–8221, 2024.
- Hao Shao, Shengju Qian, Han Xiao, Guanglu Song, Zhuofan Zong, Letian Wang, Yu Liu, and Hongsheng Li. Visual cot: Advancing multi-modal language models with a comprehensive dataset and benchmark for chain-of-thought reasoning. *Advances in Neural Information Processing Systems*, 37:8612–8642, 2024.
- Ruohong Zhang, Bowen Zhang, Yanghao Li, Haotian Zhang, Zhiqing Sun, Zhe Gan, Yinfei Yang, Ruoming Pang, and Yiming Yang. Improve vision language model chain-of-thought reasoning. In *Proceedings of the 63rd Annual Meeting of the Association for Computational Linguistics (Volume 1: Long Papers)*, pages 1631–1662, 2025.
- Jing Dong, Wei Wang, and Tieniu Tan. Casia image tampering detection evaluation database. In *2013 IEEE China summit and international conference on signal and information processing*, pages 422–426. IEEE, 2013.
- Yu-Feng Hsu and Shih-Fu Chang. Detecting image splicing using geometry invariants and camera characteristics consistency. In *2006 IEEE international conference on multimedia and expo*, pages 549–552. IEEE, 2006.
- Bihan Wen, Ye Zhu, Ramanathan Subramanian, Tian-Tsong Ng, Xuanjing Shen, and Stefan Winkler. Coverage—a novel database for copy-move forgery detection. In *2016 IEEE international conference on image processing (ICIP)*, pages 161–165. Ieee, 2016.
- Zhendong Wang, Jianmin Bao, Wengang Zhou, Weilun Wang, Hezhen Hu, Hong Chen, and Houqiang Li. Dire for diffusion-generated image detection. In *Proceedings of the IEEE/CVF International Conference on Computer Vision*, pages 22445–22455, 2023.
- You-Ming Chang, Chen Yeh, Wei-Chen Chiu, and Ning Yu. Antifakeprompt: Prompt-tuned vision-language models are fake image detectors. In *ICLR 2025 Workshop on Building Trust in Language Models and Applications*, 2025.
- Hengrui Kang, Siwei Wen, Zichen Wen, Junyan Ye, Weijia Li, Peilin Feng, Baichuan Zhou, Bin Wang, Dahua Lin, Linfeng Zhang, et al. Legion: Learning to ground and explain for synthetic image detection. In *Proceedings of the IEEE/CVF International Conference on Computer Vision*, pages 18937–18947, 2025.
- Yikun Ji, Yan Hong, Qi Fan, Huijia Zhu, Weiqiang Wang, Liqing Zhang, Jianfu Zhang, et al. Fakexplain: Ai-generated image detection via human-aligned grounded reasoning. In *The Fourteenth International Conference on Learning Representations*, 2026.
- Junyan Ye, Baichuan Zhou, Zilong Huang, Junan Zhang, Tianyi Bai, Hengrui Kang, Jun He, Honglin Lin, Zihao Wang, Tong Wu, Zhizheng Wu, Yiping Chen, Dahua Lin, Conghui He, and Weijia Li. LOKI: A comprehensive synthetic data detection benchmark using large multimodal models. In *The Thirteenth International Conference on Learning Representations*, 2025.

- Zhenglin Huang, Jinwei Hu, Xiangtai Li, Yiwei He, Xingyu Zhao, Bei Peng, Baoyuan Wu, Xiaowei Huang, and Guangliang Cheng. Sida: Social media image deepfake detection, localization and explanation with large multimodal model. In *Proceedings of the Computer Vision and Pattern Recognition Conference*, pages 28831–28841, 2025.
- Zhipei Xu, Xuanyu Zhang, Runyi Li, Zecheng Tang, Qing Huang, and Jian Zhang. Fakeshield: Explainable image forgery detection and localization via multi-modal large language models. In *The Thirteenth International Conference on Learning Representations*, 2025.
- Siwei Wen, Junyan Ye, Peilin Feng, Hengrui Kang, Zichen Wen, Yize Chen, Jiang Wu, wenjun wu, Conghui He, and Weijia Li. Spot the fake: Large multimodal model-based synthetic image detection with artifact explanation. In *The Thirty-ninth Annual Conference on Neural Information Processing Systems*, 2026.
- Hui Han, Shunli Wang, Yandan Zhao, Taiping Yao, and Shouhong Ding. Vrag-dfd: Verifiable retrieval-augmentation for mllm-based deepfake detection. *arXiv preprint arXiv:2604.13660*, 2026.
- Mude Hui, Siwei Yang, Bingchen Zhao, Yichun Shi, Heng Wang, Peng Wang, Yuyin Zhou, and Cihang Xie. Hq-edit: A high-quality dataset for instruction-based image editing. *arXiv preprint arXiv:2404.09990*, 2024.
- Haotian Liu, Chunyuan Li, Qingyang Wu, and Yong Jae Lee. Visual instruction tuning. *Advances in neural information processing systems*, 36:34892–34916, 2023.
- Haotian Liu, Chunyuan Li, Yuheng Li, Bo Li, Yuanhan Zhang, Sheng Shen, and Yong Jae Lee. Llava-next: Improved reasoning, ocr, and world knowledge, January 2024.
- Wenliang Dai, Junnan Li, Dongxu Li, Anthony Tiong, Junqi Zhao, Weisheng Wang, Boyang Li, Pascale N Fung, and Steven Hoi. Instructblip: Towards general-purpose vision-language models with instruction tuning. *Advances in neural information processing systems*, 36:49250–49267, 2023.
- Zhuosheng Zhang, Aston Zhang, Mu Li, Hai Zhao, George Karypis, and Alex Smola. Multimodal chain-of-thought reasoning in language models. *arXiv preprint arXiv:2302.00923*, 2023b.
- Junxian Li, Xinyue Xu, Sai Ma, Di Zhang, and Sichao Li. Faithful-first reasoning, planning, and acting for multimodal llms. *arXiv preprint arXiv:2511.08409*, 2025.
- Changjiang Jiang, Xinkuan Sha, Fengchang Yu, Jingjing Liu, Jian Liu, Mingqi Fang, Chenfeng Zhang, and Wei Lu. Fake-hr1: Rethinking reasoning of vision language model for synthetic image detection. In *ICASSP 2026-2026 IEEE International Conference on Acoustics, Speech and Signal Processing (ICASSP)*, pages 10482–10486. IEEE, 2026.
- Xiao Guo, Xiufeng Song, Yue Zhang, Xiaohong Liu, and Xiaoming Liu. Rethinking vision-language model in face forensics: Multi-modal interpretable forged face detector. In *Proceedings of the Computer Vision and Pattern Recognition Conference*, pages 105–116, 2025.
- Richard Zhang, Phillip Isola, Alexei A Efros, Eli Shechtman, and Oliver Wang. The unreasonable effectiveness of deep features as a perceptual metric. In *Proceedings of the IEEE conference on computer vision and pattern recognition*, pages 586–595, 2018.
- Nobuyuki Otsu. A threshold selection method from gray-level histograms. *Automatica*, 11:285–296, 1975.
- Peng Wang, Shuai Bai, Sinan Tan, Shijie Wang, Zhihao Fan, Jinze Bai, Keqin Chen, Xuejing Liu, Jialin Wang, Wenbin Ge, et al. Qwen2-vl: Enhancing vision-language model’s perception of the world at any resolution. *arXiv preprint arXiv:2409.12191*, 2024.
- Edward J Hu, yelong shen, Phillip Wallis, Zeyuan Allen-Zhu, Yuanzhi Li, Shean Wang, Lu Wang, and Weizhu Chen. LoRA: Low-rank adaptation of large language models. In *International Conference on Learning Representations*, 2022.

A Stage A: source-dataset adapters

Stage A ingests source-dataset records into the canonical `EditTriplet` schema. Each adapter handles the source dataset’s format-specific quirks; the rest of the pipeline operates on a single uniform schema thereafter. We ship two adapters with the initial release.

Pico-Banana adapter. Source format is JSONL with one record per edit, each containing fields for the input image (`local_input_image` or `open_image_input_url`), the edited image (`output_image`), the natural-language instruction (`text`), and a source-curated edit category (`edit_type`, e.g. “Remove an existing object”). The adapter:

- Constructs `triplet_id` as `picobanana_{stem}` where `stem` is the sanitized filename stem from `output_image`. We preserve the full stem rather than parsing a numeric index, because not all Pico-Banana filenames are numeric (e.g., `kewsee_retry1.png`), and the integer-only parse produced $\sim 22\%$ duplicate IDs on the full release.
- Resolves `real_path` from `local_input_image` under `dataset_root`; falls back to downloading `open_image_input_url` into a cache directory if the local file is missing and `download_missing=True`.
- Sets `provided_mask_path = None` (Pico-Banana ships no ground-truth masks; Stage B synthesizes them).
- Preserves the source `edit_type` string in metadata. Stage D consumes this for category classification rather than using it directly as the canonical label.

MagicBrush adapter. Source format is the HuggingFace `osunlp/MagicBrush` dataset, with one row per editing turn. Each row contains `source_img`, `target_img`, `mask_img` (a ground-truth manipulation mask), `instruction`, `img_id` (the COCO image id), and `turn_index` (1-based). The adapter:

- Constructs `triplet_id` as `magicbrush_{split}_{img_id}_t{turn:02d}`. The split tag prevents train/dev collisions if ingested parquets are later merged.
- Materializes `source_img`, `target_img`, and `mask_img` as PNGs under the output root and records their paths.
- Decodes MagicBrush’s mask encoding correctly: the `mask_img` field is an RGB image where the edited region is painted pure black ($[0, 0, 0]$) over the target image’s color content. The naive “`convert(L) > 127`” threshold inverts the mask. The adapter checks for all-or-mostly-black pixels pattern and inverts as needed.
- Sets `metadata[‘source_is_authentic’] = True` only for `turn_index == 1`; for turns ≥ 2 the “source” is itself a previously edited image. Downstream code requiring pristine real images filters on this flag, or sets `single_turn_only=True` at ingest time.

Adapter contract. Adding a new source dataset requires implementing a single class inheriting from `IngestionAdapter` (`adapters/base.py`) and registering it in the Hydra config. The base class handles output-parquet writing, deterministic ID generation, and image materialization; subclasses implement only the source-specific record-shape parsing.

B Forensic-prior templates

The Stage E reasoning chain includes one category-level forensic prior per triplet (Step 5), drawn from the table below by the classified edit category. Templates are versioned (`TEMPLATE_VERSION = "v1.0"`); the version is recorded in each chain’s structured header for downstream auditability. All templates are phrased as category-level facts (“edits of this type typically exhibit. . .”) rather than per-triplet observations, so the model learns to distinguish category-conditional knowledge from per-triplet evidence.

Table 4: Per-category forensic-signature priors. Each template is one or two sentences naming concrete forensic features that a detector would plausibly attend to that category.

Category	Forensic-signature template
<code>object_addition</code>	Boundary discontinuities at the edge of the inserted region, and lighting or shadow inconsistencies between the new object and its surrounding scene.
<code>object_removal</code>	Inpainting artifacts where the removed object used to be, such as blurred or repeated texture patches that disagree with the surrounding context.
<code>object_replacement</code>	Boundary mismatches at the silhouette of the new object, plus scale or perspective inconsistencies if the replacement does not match the original object’s geometry.
<code>attribute_change</code>	Color or texture discontinuities along the object’s boundary where the edited region meets its preserved surroundings, often without changes elsewhere in the image.
<code>style_transfer</code>	Global texture and brushstroke patterns are inconsistent with natural photography, applied uniformly across the image regardless of original content.
<code>photometric</code>	A global histogram shift or noise overlay applied uniformly to all pixels, with the underlying image content semantically unchanged from the original.
<code>scene_transformation</code>	Globally consistent changes in lighting, color temperature, or weather effects that affect the whole scene coherently rather than any single object.
<code>background_change</code>	A sharp transition between a preserved foreground subject and a newly-introduced background, sometimes with mismatched lighting or perspective at the boundary.
<code>text_edit</code>	Font or rendering artifacts in the modified text region — inconsistent letter spacing, mismatched typefaces, or rendering noise distinct from the original photographic text.
<code>geometric</code>	Canvas-level transformations such as cropped boundaries, scaled content, or extrapolated regions outside the original frame, rather than localized object edits.
<code>human_centric</code>	Subject-localized stylization or attribute changes confined to a person, with the surrounding scene preserved; identity-preserving transformations often introduce distinctive rendering artifacts around the face and hair.
<i>other</i>	Edit characteristics depend on the specific operation; without a confirmed category, look broadly for any local boundary discontinuities or global statistical shifts.

C Retrospective threshold-sweep tool

Stage B’s two-path scope routing depends on a threshold τ on the combined diff signal’s mean, calibrated per dataset to target a $\sim 30\%$ Path-1 global routing rate (§5.2). We provide `scripts/sweep_global_threshold.py` to surface this calibration without re-running Stage B from scratch.

What it computes. For each candidate threshold $\tau' \in T_{\text{candidates}}$, the tool computes the Path-1 global rate that would result from setting `global_mean_threshold = τ'` . The computation is exact because Stage B records each triplet’s `combined_diff_mean` alongside its scope label; recovering the Path-1 rate at any other threshold is a simple comparison.

What the tool does *not* simulate is Path 2 (the post-Otsu area-based promotion to `global`). Path 2 requires the binarized mask, which is not retained in Stage B’s per-triplet record. The reported Path-1 rate is therefore a lower bound on the resulting total global rate; for typical thresholds in our datasets the post-Otsu contribution is small (<1 percentage point).

Usage.

```
uv run python scripts/sweep_global_threshold.py \
  paths.masks_parquet=${output_root}/masks/pico_banana.parquet \
  candidate_thresholds=[0.50,0.52,0.54,0.56,0.58,0.60,0.62,0.64]
```

The output is a CSV report with columns (`threshold`, `path1_global_rate`, `n_total`). The user picks the τ that lands closest to the desired routing rate. On Pico-Banana with the LAB+LPIPS+SSIM stack, $\tau = 0.62$ produces a 30.4% Path-1 rate; this is the calibrated threshold reported in Table 2.

D Per-category chain examples

We show one example reasoning chain per canonical category. Each example is a Stage E output verbatim, with the triplet’s instruction quoted in Step 1. The structured header on the first line records category, scope, difficulty bin, and the source of the category classification. Steps 1–4 and Step 6 are triplet-grounded; Step 5 is the category-level forensic prior from Appendix B.

The chains are short (~80–150 words each); we present them without surrounding prose, so the format and the within-step variation across categories are directly comparable.

object_addition

[category=object_addition, scope=local, difficulty=easy, source=rule_based]

1. The edit instruction states: “add a polar bear”.
2. The mask of changed pixels covers roughly 12% of the image and is concentrated in the lower-left region.
3. Structural change relative to the original is minor (SSIM-based score = 0.09), and the edit region is well-concentrated in a single coherent region.
4. The edit is classified as object_addition, inferred from the instruction text via a rule-based keyword match (confidence 0.80).
5. Edits of this type typically exhibit boundary discontinuities at the edge of the inserted region, and lighting or shadow inconsistencies between the new object and its surrounding scene.
6. Overall, this triplet is easier than average to detect, given clear local geometry and a low-complexity instruction (difficulty score = 0.11, instruction complexity = 0.12).

object_removal

[category=object_removal, scope=local, difficulty=medium, source=rule_based]

1. The edit instruction states: “get rid of the framed pictures”.
2. The mask of changed pixels covers roughly 17% of the image and is centered in the image.
3. Structural change relative to the original is minor (SSIM-based score = 0.15), and the edit region is moderately concentrated.
4. The edit is classified as object_removal, inferred from the instruction text via a rule-based keyword match (confidence 0.85).
5. Edits of this type typically exhibit inpainting artifacts where the removed object used to be, such as blurred or repeated texture patches that disagree with the surrounding context.
6. Overall, this triplet is of moderate detection difficulty (difficulty score = 0.21, instruction complexity = 0.06).

object_replacement

[category=object_replacement, scope=local, difficulty=hard, source=rule_based]

1. The edit instruction states: “replace the stuffed animals with a pillow.”.
2. The mask of changed pixels covers roughly 40% of the image and is centered in the image.
3. Structural change relative to the original is moderate (SSIM-based score = 0.32), and the edit region is well-concentrated in a single coherent region.
4. The edit is classified as object_replacement, inferred from the instruction text via a rule-based keyword match (confidence 0.85).
5. Edits of this type typically exhibit boundary mismatches at the silhouette of the new object, plus scale or perspective inconsistencies if the replacement does not match the original object’s geometry.
6. Overall, this triplet is harder than average to detect, given diffuse geometry or a high-complexity instruction (difficulty score = 0.28, instruction complexity = 0.15).

attribute_change

[category=attribute_change, scope=local, difficulty=easy, source=rule_based]

1. The edit instruction states: “let the apples be changed to orange slices”.
2. The mask of changed pixels covers roughly 13% of the image and is concentrated in the lower-right region.
3. Structural change relative to the original is minor (SSIM-based score = 0.12), and the edit region is well-concentrated in a single coherent region.
- x 4. The edit is classified as attribute_change, inferred from the instruction text via a rule-based keyword match (confidence 0.80).
5. Edits of this type typically exhibit color or texture discontinuities along the object’s boundary where the edited region meets its preserved surroundings, often without changes elsewhere in the image.
6. Overall, this triplet is easier than average to detect, given clear local geometry and a low-complexity instruction (difficulty score = 0.10, instruction complexity = 0.08).

style_transfer

[category=style_transfer, scope=global, difficulty=hard, source=dataset_label]

1. The edit instruction states: “enhance the image to a modern aesthetic by applying a vibrant, high-contrast color grade with crisp details, brightening the overall scene, and subtly smoothing any visible wear or rust on the bridge.”.
2. The mask of changed pixels covers roughly 100% of the image and spans the entire image.
3. Structural change relative to the original is substantial (SSIM-based score = 0.80), and the edit region is well-concentrated in a single coherent region.
4. The edit is classified as style_transfer, based on the dataset’s curated edit-type label.
5. Edits of this type typically exhibit global texture and brushstroke patterns inconsistent with natural photography, applied uniformly across the image regardless of original content.
6. Overall, this triplet is harder than average to detect, given diffuse geometry or a high-complexity instruction (difficulty score = 0.56, instruction complexity = 0.58).

photometric

[category=photometric, scope=global, difficulty=medium, source=dataset_label]

1. The edit instruction states: “colorize the black and white image realistically, depicting natural skin tones, jungle foliage, and gear colors, then subtly shift the overall color temperature towards a cooler tone.”.
2. The mask of changed pixels covers roughly 100% of the image and spans the entire image.
3. Structural change relative to the original is substantial (SSIM-based score = 0.64), and the edit region is well-concentrated in a single coherent region.
4. The edit is classified as photometric, based on the dataset’s curated edit-type label.
5. Edits of this type typically exhibit a global histogram shift or noise overlay applied uniformly to all pixels, with the underlying image content semantically unchanged from the original.
6. Overall, this triplet is of moderate detection difficulty (difficulty score = 0.48, instruction complexity = 0.67).

scene_transformation

[category=scene_transformation, scope=local, difficulty=medium, source=rule_based]

1. The edit instruction states: “let the cabinets be made of dark wood”.
2. The mask of changed pixels covers roughly 13% of the image and is centered in the image.
3. Structural change relative to the original is minor (SSIM-based score = 0.10), and the edit region is moderately concentrated.
4. The edit is classified as scene_transformation, inferred from the instruction text via a rule-based keyword match (confidence 0.65).
5. Edits of this type typically exhibit globally consistent changes in lighting, color temperature, or weather effects that affect the whole scene coherently rather than any single object.
6. Overall, this triplet is of moderate detection difficulty (difficulty score = 0.19, instruction complexity = 0.08).

background_change

[category=background_change, scope=local, difficulty=easy, source=rule_based]

1. The edit instruction states: “it should be a mountain in the background.”
2. The mask of changed pixels covers roughly 10% of the image and is concentrated in the lower-right region.
3. Structural change relative to the original is minor (SSIM-based score = 0.07), and the edit region is moderately concentrated.
4. The edit is classified as background_change, inferred from the instruction text via a rule-based keyword match (confidence 0.75).
5. Edits of this type typically exhibit a sharp transition between a preserved foreground subject and a newly-introduced background, sometimes with mismatched lighting or perspective at the boundary.
6. Overall, this triplet is easier than average to detect, given clear local geometry and a low-complexity instruction (difficulty score = 0.13, instruction complexity = 0.08).

text_edit

[category=text_edit, scope=local, difficulty=hard, source=rule_based]

1. The edit instruction states: “change the text on the parking meter to say “NO”.”
2. The mask of changed pixels covers roughly 8% of the image and is centered in the image.
3. Structural change relative to the original is minor (SSIM-based score = 0.02), and the edit region is diffuse or split across multiple sub-regions.
4. The edit is classified as text_edit, inferred from the instruction text via a rule-based keyword match (confidence 0.70).
5. Edits of this type typically exhibit font or rendering artifacts in the modified text region — inconsistent letter spacing, mismatched typefaces, or rendering noise distinct from the original photographic text.
6. Overall, this triplet is harder than average to detect, given diffuse geometry or a high-complexity instruction (difficulty score = 0.24, instruction complexity = 0.18).

geometric

[category=geometric, scope=local, difficulty=hard, source=rule_based]

1. The edit instruction states: “make the piece of paper hanging on the wall a mirror”.
2. The mask of changed pixels covers roughly 14% of the image and is concentrated in the upper-left region.
3. Structural change relative to the original is minor (SSIM-based score = 0.08), and the edit region is diffuse or split across multiple sub-regions.
4. The edit is classified as geometric, inferred from the instruction text via a rule-based keyword match (confidence 0.85).
5. Edits of this type typically exhibit canvas-level transformations such as cropped boundaries, scaled content, or extrapolated regions outside the original frame, rather than localized object edits.
6. Overall, this triplet is harder than average to detect, given diffuse geometry or a high-complexity instruction (difficulty score = 0.23, instruction complexity = 0.19).

human_centric

[category=human_centric, scope=global, difficulty=hard, source=dataset_label]

1. The edit instruction states: “transform the main subject (the person playing the flute) into a detailed, expressive black ink line-art sketch, utilizing varied line weights to highlight facial features, the texture of the cap.”
2. The mask of changed pixels covers roughly 100% of the image and spans the entire image.
3. Structural change relative to the original is substantial (SSIM-based score = 0.72), and the edit region is well-concentrated in a single coherent region.
4. The edit is classified as human_centric, based on the dataset’s curated edit-type label.
5. Edits of this type typically exhibit subject-localized stylization or attribute changes confined to a person, with the surrounding scene preserved; identity-preserving transformations often introduce distinctive rendering artifacts around the face and hair.
6. Overall, this triplet is harder than average to detect, given diffuse geometry or a high-complexity instruction (difficulty score = 0.51, instruction complexity = 0.58).

other

```
[category=other, scope=local, difficulty=medium, source=fallback]
```

1. The edit instruction states: “have there be a basket of fruit on the counter.”.
2. The mask of changed pixels covers roughly 8% of the image and is centered in the image.
3. Structural change relative to the original is minor (SSIM-based score = 0.06), and the edit region is moderately concentrated.
4. The edit is classified as other, could not be determined confidently from the available signals; treated as an unspecified edit type.
5. Edits of this type typically exhibit edit characteristics that depend on the specific operation; without a confirmed category, look broadly for any local boundary discontinuities or global statistical shifts.
6. Overall, this triplet is of moderate detection difficulty (difficulty score = 0.16, instruction complexity = 0.10).

E Qualitative mask examples

Figures 3 and 4 compare EditSleuth’s Stage B masks against MagicBrush’s ground-truth manipulation masks across nine representative edit categories. EditSleuth’s masks consistently localize the edited region, including multi-component edits (e.g., the two removed picture frames in `object_removal` and the two-region `scene_transformation`). Their boundaries are morphologically rougher than the ground truth’s: derived from thresholded pixel-difference signals rather than learned segmentation, EditSleuth masks follow the local texture of the diff signal and exhibit irregular outlines and occasional small false-positives in texture-heavy regions (most visibly in the `text_edit` row).



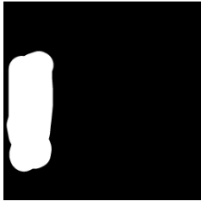





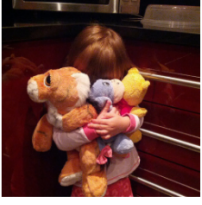
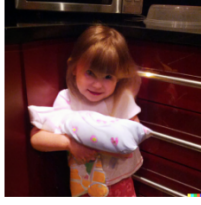


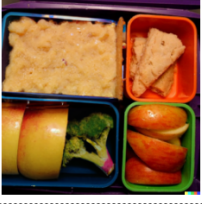



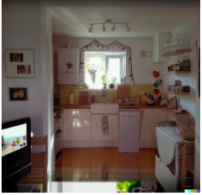
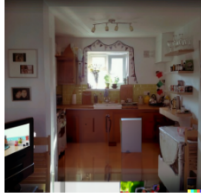


Category	Original Image	Edited Image	Ground Truth Mask	EditSleuth Mask
object_addition				
object_removal				
object_replacement				
attribute_change				
scene_transformation				

Figure 3: Examples of the original images, edited images, ground-truth masks, and generated masks from EditSleuth for categories object_addition, object_removal, object_replacement, attribute_change, and scene_transformation.







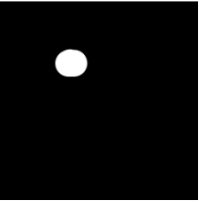



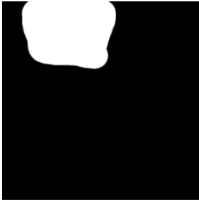



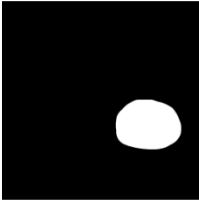

Category	Original Image	Edited Image	Ground Truth Mask	EditSleuth Mask
background_change				
text_edit				
geometric				
other				

Figure 4: Examples of the original images, edited images, ground-truth masks, and generated masks from EditSleuth for categories background_change, text_edit, geometric, and other.